Enhancing the load-bearing capacity of footings on saturated sand slopes using Geocell reinforcement

Manesht Maleki Vasegh[a], Vahid Rostami[b,*], Hamid Reza Rabieifar[c]

[a]Department of Civil Engineering, Ki.C., Islamic Azad University, Kish, Iran

[b]Department of Civil Engineering, Ha.C., Islamic Azad University, Hamedan, Iran

[c]Department of Civil Engineering, STB, Islamic azad university, Tehran, Iran

(Communicated by Asadollah Aghajani)

Abstract

This research paper focuses on the load-bearing capacity of strip footings constructed on Geocell-reinforced sand slopes. The study included various experiments and numerical simulations to investigate the behavior of Geocell reinforcement when subjected to bending loads. The results indicated that when the height of the Geocell increased, the deep beam behavior was more pronounced, which suggests that the Geocell layer can act effectively as a deep beam. Additionally, the study revealed that when eccentric loading is applied to foundations near the sand slope crest, it decreases the footing's initial bearing capacity. When altering the geometry of a sand slope is not feasible and modifying the geotechnical properties of the soil is either impractical or expensive, the implementation of appropriate soil reinforcement can prove to be beneficial. Lastly, the findings of the study suggest that an increase in the number of Geocells can bring the foundation's load-bearing capacity closer to the loading capacity of a foundation on horizontal ground.

Keywords: load-bearing capacity, strip footings, geocell, reinforced sand slope, saturated sand
2020 MSC: 00A06, 62P30

1 Introduction

Unreinforced soils generally exhibit satisfactory performance under compression, but they often lack significant tensile strength. As a result, reinforcing these soils becomes necessary to enhance their tensile performance. By introducing reinforcement techniques, the overall strength and stability of the soil can be improved, ensuring better performance under tension and reducing the risk of failure. Reinforcing soil serves the purpose of enhancing its stability, increasing its load-bearing capacity, and reducing settlement and lateral deformation, as mentioned by Oghabi et al. [12]. When a footing is placed on a sand slope, it not only diminishes the load-bearing capacity but also significantly raises the risk of failure. It is crucial to consider these factors when designing and constructing footings on sandy slopes to ensure the safety and structural integrity of the foundation. In situations where certain structures, such as bridges, require foundations to be constructed near or on sand slopes, it is crucial to carefully consider material specifications

and sand slope geometry. Inadequate attention to these factors can result in complete slope failure or insufficient bearing capacity within the foundation. Therefore, it is essential to conduct thorough geotechnical investigations and engineering analyses to ensure the stability and safety of the foundation in such scenarios. When altering the geometry of a sand slope is not feasible and modifying the geotechnical properties of the soil is either impractical or expensive, the implementation of appropriate soil reinforcement can prove to be beneficial [13]. Various studies have been conducted on reinforced soil slopes, specifically focusing on the impact of reinforcement length and distance on the behavior of these slopes. In order to thoroughly understand the failure mechanism of geosynthetic-reinforced soil slopes and assess the validity of design hypotheses and methods for such walls, both numerical and experimental studies have been undertaken. These investigations have highlighted that the failure surface differs from the propagation of the failure region. Instead, its location is dependent on factors such as the geometry, strength, and stiffness of the reinforcement elements [2, 7, 9, 10, 14, 18]. By reinforcing the soil, its strength and stability can be improved, mitigating potential issues associated with the existing slope geometry and soil characteristics. Soil stabilization techniques involve various methods such as soil improvement, preloading, piling, and the utilization of geosynthetics. Among these methods, the use of geosynthetics for soil levelling has gained significant popularity. Soil reinforcement is achieved by incorporating strong materials into the soil to enhance its mechanical characteristics. For effective reinforcement, these materials should possess appropriate tensile strength, minimal strain hardening, and excellent durability in the soil environment. The increased utilization of polymers in soil stabilization has led to the emergence of innovative geosynthetic products like geocells in the market. Incorporating geocells into unreinforced soil can yield significant improvements in soil shear strength and settlement reduction. One notable advantage of geocells, when compared to other geosynthetic materials, is their three-dimensional structure. This unique characteristic enhances soil strength not only by increasing the shear strength between the soil and the reinforcing element but also by enhancing the compressive strength of the soil behind the vertical wall of the reinforcing element. Essentially, a slope reinforced with geocells behaves like a beam within the soil due to the geocell's height and flexural properties. This results in reduced displacement and increased safety factors for the slope, as highlighted by Mehdipour et al. [6, 11].

The use of geocells as a reinforcement method has a wide range of applications in civil projects due to their effectiveness and efficiency. Geocell-reinforced soil is primarily used to withstand static and cyclic loads. It is commonly employed to increase the load-bearing capacity of soft soil and decrease settlement and displacements of slopes. Geocells act as a layer, confining the soil and preventing it from moving outward of the loaded region. This confinement also helps reduce soil swelling, resulting in changes in the factor of safety of slopes. Geocells enhance the bending, tensile, and shear strengths of the soil. Additionally, due to their height, they function as a beam, providing moment of inertia and consequently improving bending strength. While the bending stiffness of geocell-reinforced soil may be relatively low compared to its thickness, it can still significantly reduce deformations in different soil layers and contribute to the overall settlement reduction of the soil-structure system [3].

In the past few decades, researchers have primarily focused on investigating the load-bearing capacity of foundations on horizontally reinforced ground using geosynthetics. However, there have been relatively fewer studies conducted on the load-bearing capacity of (sand/earth) slopes. Fakher and Jones [5] conducted a study to examine the impact of bending stiffness on geogrid reinforcement using FLAC software. Their findings revealed that despite the relatively low bending stiffness in relation to the thinness of the geogrid layer, it played a crucial role in reducing the deformation of the geogrid layer. As a result, this decrease in deformation contributed to the overall reduction in settlement of the system. The study conducted by [16, 17] focused on simulating the performance of geocell reinforcement. In their simulations, they took into account the resistance of the contact surface between the soil and geocell. They assumed the geocell reinforcement to behave like a beam on an elastic bed. In the study conducted by Dash et al. [4], they carried out experiments to examine the behavior of a geocell layer under bending conditions. They found that the geocell layer exhibited characteristics similar to those of a beam when subjected to flexural stresses.

The researchers discovered that as the height of the geocell layer increased, the deep beam behavior became more pronounced in the geocell layer. This suggests that the geocell layer can effectively function as a deep beam when subjected to bending loads. Overall, the findings of Dash et al.'s study provide valuable insights into the behavior of geocell layers and their potential applications in engineering and construction projects. Honardar and Roshanzamir [8] conducted a study using PLAXIS to examine the load-bearing capacity of strip foundations placed on geogrid-reinforced ground under eccentric loading, as well as unreinforced slopes [15]. They analyzed the impact of various factors, including foundation depth, distance between foundation edge and slope crest, slope geometry parameters, and loading eccentricity, on the load-bearing capacity. The analytical findings of Honardar and Roshanzamir [8] indicated that when eccentric loading is applied to foundations with eccentricity directed towards the slope crest, it results in a reduction in the bearing capacity of the foundation. Conversely, when eccentric loading is applied to foundations near the slope crest, where eccentricity is directed away from the crest, it leads to an initial increase in

the foundation's bearing capacity, followed by a gradual decrease. Another influential parameter is the depth of the foundation. Increasing the foundation depth enhances the loading capacity of the foundation adjacent to a slope, bringing it closer to the loading capacity of a foundation on horizontal ground. The researchers utilized FLAC 3D, a finite element analysis software, for modelling purposes, and compared their numerical findings with laboratory test results. The study revealed that an increase in the number of geogrids enhances the bond between soil particles and the cohesion between soil particles and geogrids. Consequently, this leads to a larger load distribution area and an increase in the ultimate load-bearing capacity. Specifically, the load-bearing capacity was found to increase with the addition of three geogrids. However, further increments in the number of geogrids did not significantly enhance the loading capacity.

The authors conducted laboratory tests to investigate the load-bearing capacity of geocell-reinforced strip footings when constructed near saturated sand slopes and to validate the correction of the results of the study. This investigation includes the Plaxis model. This study aimed to assess the impact of various parameters on the footing's load-bearing capacity. These parameters included geocell width, geocell height, geocell distance from the foundation level, and the angle of the sand slope. It is important to note that geocells as 3D elements for soil levelling have not been previously modelled in laboratory settings, hence the motivation for this research.

2 Test plan

In order to accomplish the objectives, a total of 111 experimental series were conducted. The focus of these experiments was on the stress-strain behavior of the reinforced soil, with particular emphasis on the geocell width and its distance from the foundation level. The test plan was designed to specifically address these two influential parameters. Table 1 identifies the series of tests conducted.

Table 1: Summarized test plan

Test series	Type of reinforcement	u/B	b/B	i	No. of the test
1	Unreinforcement	...	...	$15°, 20°, 25°$	3
2	Geocell reinforced (type G1)	0.25, 0.5, 0.75	2, 3, 5	$15°, 20°, 25°$	27
3	Geocell reinforced (type G2)	0.25, 0.5, 0.75	2, 3, 5	$15°, 20°, 25°$	27
4	Geocell reinforced (type G3)	0.25, 0.5, 0.75	2, 3, 5	$15°, 20°, 25°$	27
5	Geocell reinforced (type G4)	0.25, 0.5, 0.75	2, 3, 5	$15°, 20°, 25°$	27

3 Materials specification

In the laboratory experiments, poorly graded silica sand was used as the soil. The grading curve of this sand is shown in Figure 1, and Table 2 provides additional characteristics of the soil. The load-bearing capacity of the soil is primarily influenced by the internal friction angle and cohesion coefficient, which are crucial parameters. This study focused on determining these parameters, placing particular emphasis on their significance. To determine the internal friction angle and cohesion coefficient, direct shear tests were conducted. The initial round of tests demonstrated satisfactory repeatability in determining the internal friction angle, which was consistently measured at 28 degrees. Cohesion also played a significant role in the load-bearing capacity of the small-scale laboratory models, and it was determined to be zero. To ensure accuracy in the tests, all experiments were conducted with low vertical loading velocities. This approach aimed to minimize any potential errors and enhance the precision of the results obtained.

Table 2: Sand properties

Soil Type	Density	Internal angle (φ)	Soil Cohesion	Density ratio
Sand	$1.32 gr/cm^3$	28	0	50%

4 Test apparatus

To conduct the tests, a small-scale loading apparatus was utilized. This apparatus was specifically designed for this purpose at the Soil Mechanics Laboratory of Islamic Azad University in Hamedan. Figure 2 illustrates the components of this apparatus, which include:
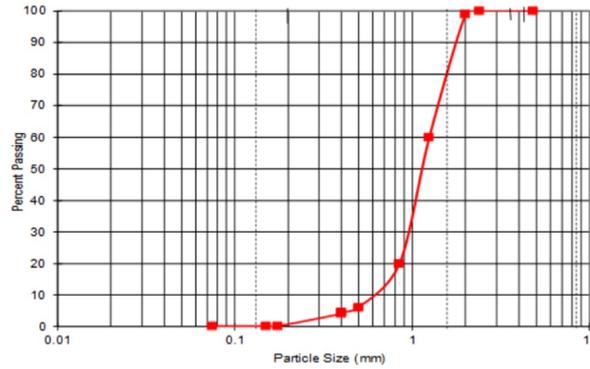
Figure 1: Grading curve of the tested sand

Figure 2: Test apparatus

a. The soil tank used in the experiment measures $50 \times 50 times 50 cm$ (inner diameters) and serves as the primary component of the apparatus for modelling the sand slope. The dimensions of the tank were selected based on prior studies to fulfil the objectives of the analysis. Key parameters influencing the box dimensions include the width of the loading plate (foundation), the additional stresses induced in the soil at various depths during foundation loading, and the confining effects near the vertical boundaries of the tank. Boussinesq [1] provided a solution for the stress distribution resulting from a load applied to the surface of a soil mass. Variations in $\Delta\sigma/q_0$ beneath a square loaded area of dimensions $B \times B$ and stress isobars can be plotted as follows. Referring to Figure 3, the presence of isobars in Boussinesq's theory indicates that the excess stress generated at a depth greater than 6B for a strip footing is less than 1% of the initial stress. Similarly, for a square footing, at a depth exceeding 2B, the excess stress reduces to less than 90% of the initial stress. Based on this figure, it can be concluded that at a distance of B from the edge of the footing, the stress increase reduces to less than 5% of the stress beneath the footing. Analogously, at a depth of 3.2B, the stress increase also diminishes to less than 5% of the stress beneath the footing. Accordingly, the lateral distance of the tank walls from the footing centre should be greater than 1.5B, and the vertical distance from the tank base to the footing should exceed 3.2B. Furthermore, another factor to consider is the extent of soil failure wedges. Depending on the soil's friction angle, these wedges can extend to a depth of approximately 2B below the footing and laterally up to 3B from the footing's edge.

To ensure sufficient rigidity and minimize tank deformation, the distance between the boundaries (container walls) and the foundation should be considered sufficiently large to avoid influencing the results. The tank is constructed using thick sheet metal. Three sides of the tank are made of sheet metal, while the fourth side is made of glass to allow for observation of soil deformation. The tank is completely filled with water and equipped with a discharge valve at its base. The preparation of the model involves initially filling the tank with water and allowing it to remain undisturbed for 24 hours. After this period, the water is drained using the valve, leaving behind saturated soil within the tank.

b. Loading System: Loading is applied via a high-precision gearbox jack with a loading capacity of 0.5 tons.

c. Footing (Foundation) Model: This model must be sufficiently rigid to realize the plane strain condition, and
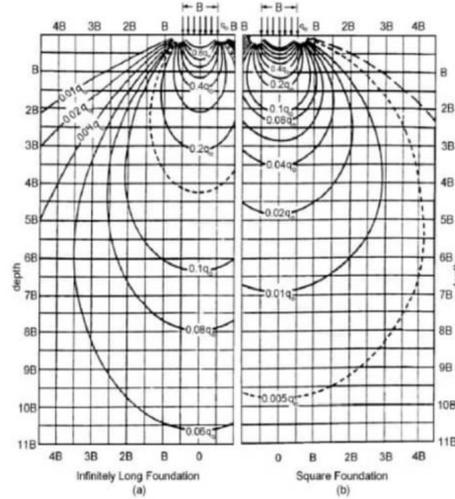
Figure 3: Pressure contours (stress isobars) based on Boussinesq's [1] theory for square and strip footings

sufficiently light so that it would induce low initial stresses on the soil and be easy to handle. The width of the footing model was selected as 5 cm (with due regard of the length of the soil container) for reducing the wall effect as well as forming complete sliding wedges. To maintain rigidity, a thickness of 2.5 cm was considered for the footing model. The length of the model was taken as 30 cm in proportion to the soil tank width.

d. Force Calculation System: This system comprised a load cell (capacity = 0.5 ton) and a digital force indicator with adjusting and calibration possibilities.

e. Strain Gauges: A deflection gauge (accuracy = 0.001mm) was used for controlling deformations under the footing model.

f. Water Supply System for Saturating the Specimen: A 20-litre water tank was mounted above the test apparatus for supplying water at equal flow rates to four different points inside the soil specimen through four pipes.

5 Building the Geocell grid

To form a geocell grid, Rockshield geogrid sheets were adhered together using the method proposed by [4]. This technique was employed to ensure the proper formation and stability of the geocell grid structure.

6 Test procedure

In order to achieve consistent compaction, the soil was systematically added to the soil tank in layers at a constant precipitation rate. Two templates, proportionate to the model's geometry, were positioned on either side of the tank. The sand was poured into the tank using the precipitation method until it reached a level equal to D-u, where D is the total height of the tank, and u is the depth of geocell placement. Subsequently, the geocell grid was placed on top of the specimen, and the sand pouring process was repeated until the desired height was attained. After placement, careful levelling was then conducted to ensure a uniformly flat soil surface for the placement of the model footing. The soil tank was then gently moved to its designated position under the loading frame, without exerting any pressure on the soil. To saturate the sand, a controlled laminar water flow, without applying pressure, was introduced into the tank, fully submerging the specimen. The specimen was left undisturbed for a period of 24 hours. Gradual loading was then applied to the model footing, maintaining a loading rate of 1mm per minute to ensure static loading conditions. This loading process continued until the foundation (footing) settled 15mm into the soil. Throughout the loading procedure, the corresponding values of each load and its respective settlement were meticulously recorded.

7 Model geometry

The laboratory testing involved a strip footing (with a width denoted as B) placed on a saturated sand slope. Figure 4 provides the geometrical specifications of the model. The load-bearing capacity of the footing was examined under various conditions after incorporating a geocell grid beneath it. The resulting values were then compared. To evaluate the findings, the following dimensionless parameters were utilized: the ratio of the geocell grid distance from the foundation level to the footing width (u/B), the ratio of geocell grid width to footing width (L/B), the ratio of geocell grid height to footing width (H/B), the ratio of geocell grid dimension to footing width (S/B), the ratio of geocell height to footing width (h/B), and the sand slope angle. To compare the outcomes between reinforced and unreinforced cases, the bearing capacity ratio (BCR) was employed. BCR represents the ratio of the reinforced bearing capacity to the unreinforced bearing capacity and can be calculated as follows:

$$BCR = q_r/q_{un}. \tag{7.1}$$

The BCR parameter is determined by comparing the load-bearing capacity of the strip footing on the reinforced sand bed (q_r) to the unreinforced soil bearing capacity (q_{un}) at the desired settlement. In this study, all tests were conducted until a settlement of 15mm was reached for the model in the soil. The BCR parameter was then calculated for each geocell, considering the same settlement, at sand slope angles of 15, 20, and 25 degrees.
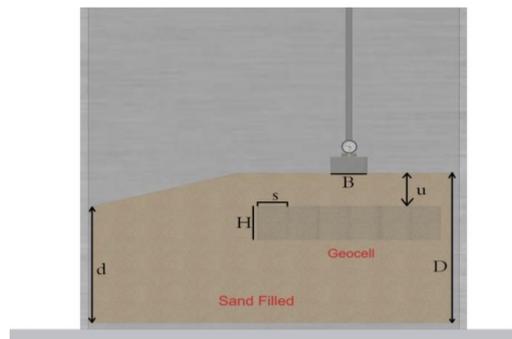

Figure 4: Schematic of test setup

8 Geocell types

In this study, four distinct types of geocells with varying geometries were utilized. These geocells were prepared following the methodology suggested by Dash et al. [4], as outlined in Table 3, where H = Height of Geocell, B = Width of Geocell, s = Pocket Size.

Table 3: Characteristics of the geocell grid used for the tests

Geocell Type			
G4	G3	G2	G1
$H = B/2$	$H = B/2$	$H = B$	$H = B$
$s = B$	$s = B/2$	$s = B$	$s = B/2$

9 Model validation

PLAXIS^{3D} is a 3-dimensional finite element program, utilized for deformation and stability analysis of the geotechnical quandaries. The simulation involved the utilization of PLAXIS^{3D}, a finite element software, incorporating geocell reinforcement. In this study, the soil was simulated using the Mohr-Coulomb constitutive model. Input parameters for the soil elements included a Young's Modulus (E) of 5 MPa, a poison's Ratio (v) of 0.3, a friction angle (ϕ) of 28°, cohesion (c) of 0 kPa, and a dry density (ρ_d) of 1450 kg/m^3 and saturated density (ρ_{sat}) of 1600 kg/m^3, and for Geocell (EA) of $1.523 \times 10^6 kN/m$ was chosen. These parameters were derived from laboratory static triaxle tests. The soil domain was discretized using 8-node hexahedral elements. The interaction between the geocell elements and the surrounding soil was modelled using interface elements, governed by the Mohr-Coulomb failure criterion.

10 Results

In order to compare the BCR curves for genotypes G1 to G4, we conducted an analysis to examine the impact of each parameter on the load-bearing capacity. This analysis was performed at various slope angles while keeping the other parameters constant at their respective optimum values. By isolating the effect of each parameter, we were able to assess its influence on the load-bearing capacity and draw meaningful comparisons between the different genotypes.

10.1 Effect of geocell layer width

Based on the diagrams presented in Figure 5, it can be observed that increasing the width of the geocell grid generally leads to an increase in the load-bearing capacity. This is because the geocell grid acts as a rigid slab, effectively redistributing the applied loads over a larger area and preventing the development of failure zones. However, upon closer examination of these diagrams, it is evident that, at a constant angle, the bearing capacity ratio (BCR) at $L/B = 3$ is consistently higher than that at $L/B = 2$. This suggests that beyond a certain limit, further improvements in load-bearing capacity may become negligible. In this study, we have identified a geocell width of 3B as the effective width, as it significantly enhances the load-bearing capacity of the soil. Considering economic constraints and the diminishing rate of load-bearing capacity improvement at larger widths, it is not economically justifiable to increase the geocell width beyond this limit.
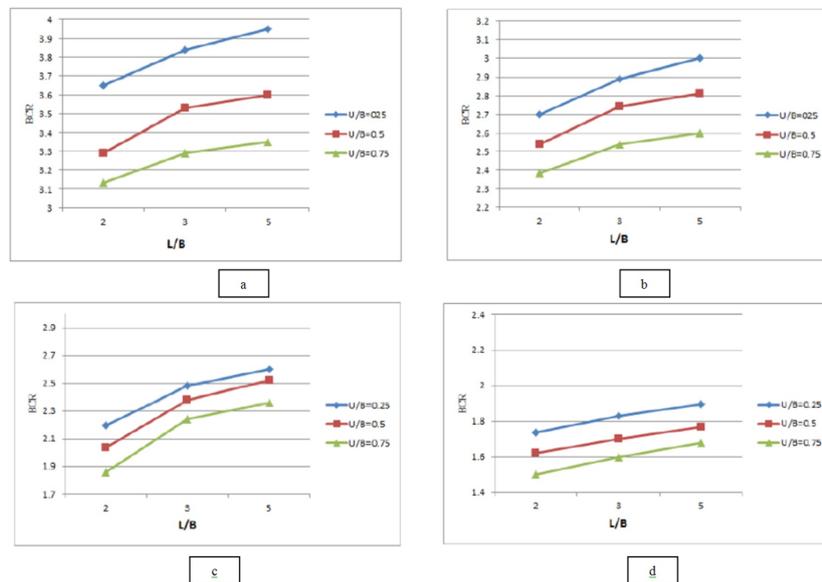

Figure 5: Variations of BCR with geocell grid distance from the footing level at different geocell widths and optimum angle (15 deg) obtained for: a) Geocell G1, b) Geocell G2, c) Geocell G3, and 4) Geocell G4.

10.2 Geocell distance from foundation level

Upon analyzing the diagrams presented in Figure 6, it is evident that increasing the distance of the geocell from the foundation level leads to a decrease in the load-bearing capacity. The maximum loading capacity was observed at the initial tested distance, specifically when the ratio of geocell distance to footing width (u/B) was 0.25.

When the embedded depth of the geocell layer is increased, it actually diminishes the effectiveness of the geocell in enhancing soil properties. This is because the soil between the footing and the geocell layer becomes compressed, resulting in increased settlements [4]. Additionally, the soil situated on the surface between the geocell and the footing can undergo lateral extension more easily.

10.3 Effect of sand slope angle

The data presented in Figure 7 demonstrates a consistent decrease in the bearing capacity ratio (BCR) as the sand slope angle increases. This indicates that the stability of the sand slope decreases, resulting in reduced load-bearing capacity. Specifically, as depicted in Figure 7a, an increase in the angle from 15 degrees to 20 degrees corresponds to a 10% reduction in the load-bearing capacity.
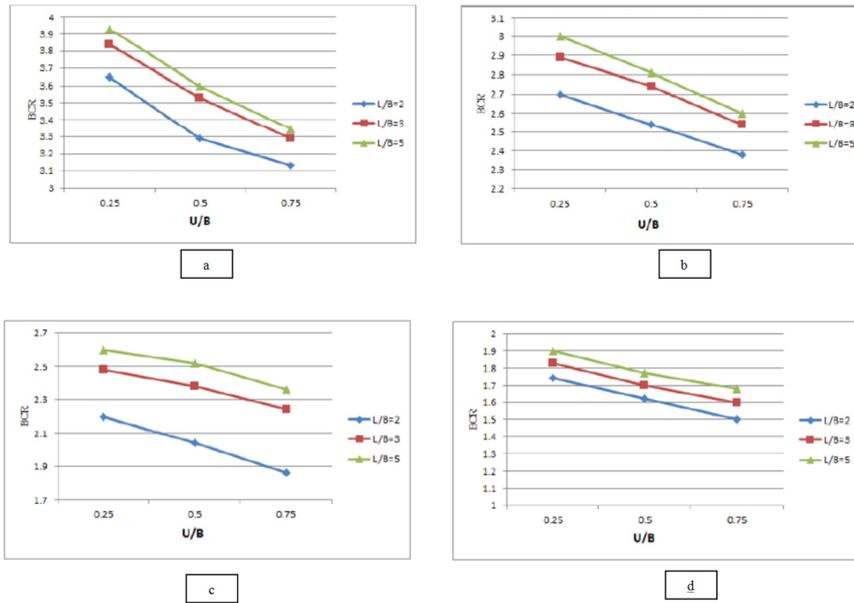
Figure 6: Variations of BCR with geocell depth (distance from foundation level) at different geocell grid widths and optimum angle (15 deg) obtained for: a) Geocell G1, b) Geocell G2, c) Geocell G3, and 4) Geocell G4.
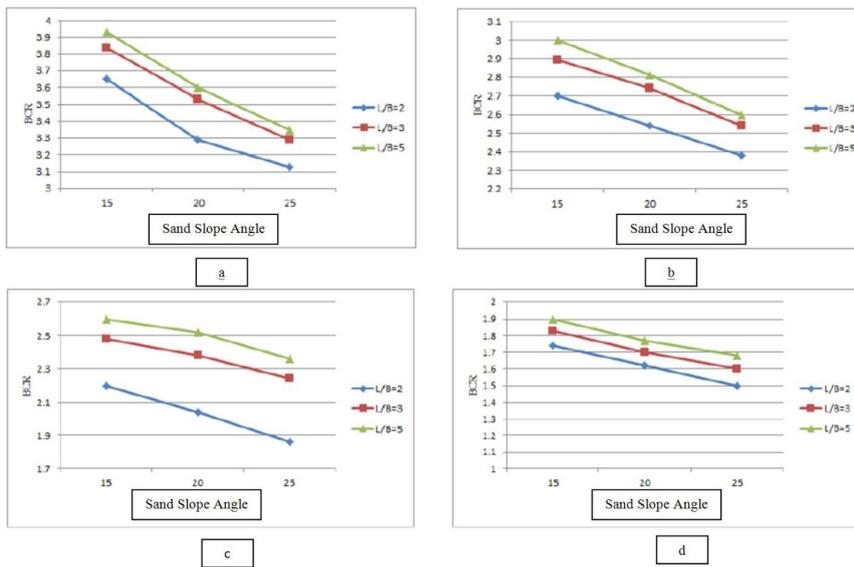

Figure 7: Variations of BCR with sand slope at different geocell grid widths and optimum embedment depth (U=0.25)

11 Validation

The numerical mesh model was generated using PLAXIS^{3D}, as depicted in Figure 8. To ensure an accurate comparison through numerical simulation, the full dimensions of the soil model in this study were utilized: 0.3 meters for the width of the slope crown, the length of the model is 0.5 meters and 3 different angles. The finite-element analysis simulation of this model can be deemed as reliable and precise. Figure 9 illustrates the Geocell model in PLAXIS^{3D}. Displacement control was employed at the centre of the slope crown surface of the model, and it was considered at the settlement of 0.015 m. Figure 10 depicts the bearing capacity of the model in 0.015 meters in 2 different phases: (1) when the model was unreinforced, and (2)a reinforced model.

As it is shown in Figure 11a, when the slope is unreinforced by applying force on it, the settlement will be higher than that of the reinforced one (Figure 11b).
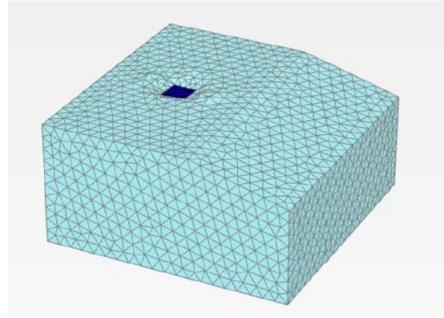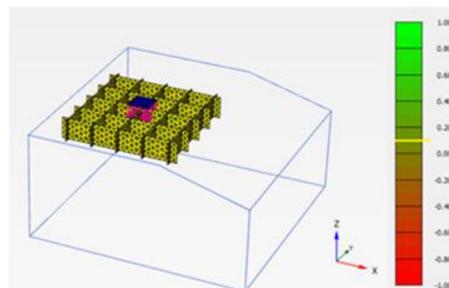
Figure 8: Meshed model

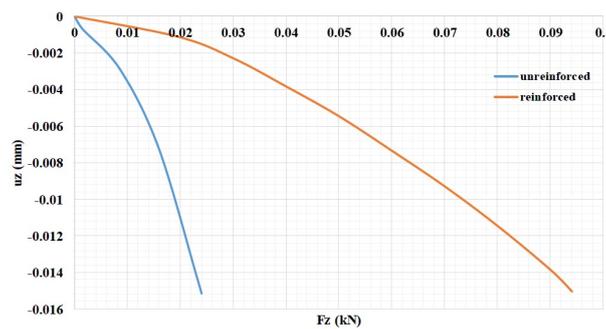Figure 9: Geocell numerical model

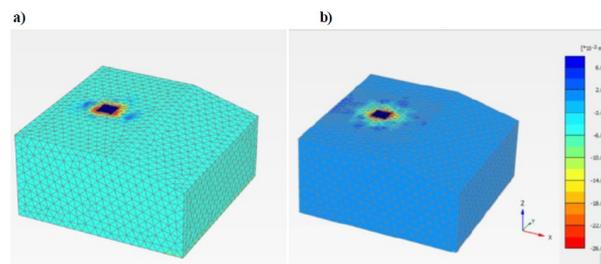Figure 10: Stress Distribution of unreinforced and reinforced model in 0.015m settlement.

Figure 11: Total displacement of model a) unreinforced, b) reinforced

12 Conclusions

In our laboratory study, we aimed to examine the impact of geocells on enhancing the load-bearing capacity of a strip footing positioned near a saturated sand slope. The key findings from our research are as follows:

1. Based on the test results, it was determined that the optimal buried reinforcement depth, where the load-bearing capacity is maximized, was found to be u/B=0.25.
2. The increase in geocell width to 5B resulted in an increase in loading capacity. However, it was observed that this increase varied across the different cases studied. As a result, a width of L/B=3 was determined to be the

optimal choice.

3. Increasing sand slope angle led to decreased load-bearing capacity.

4. Overall, the greatest load bearing capacity was obtained as 3.93, occurring at u/B=0.25, L/B=5B, and a sand slope angle of 15 deg. The least load bearing capacity was obtained as 1.5 at u/B=0.75, L/B=2B, and sand slope angle=25 deg.

References

[1] J. Boussinesq, *Application des Potentiels, à L'étude de L'équilibre et du Mouvement des Solides Élastiques: Principalement au Calcul des Déformations et des Pressions que Produisent, dans ces Solides, des Efforts Quelconques Exercés sur une Petite Partie de Leur Surface ou de Leur Intérieur: Mémoire Suivi de Notes Étendues sur Divers Points de Physique, Mathematique et d'Analyse*, Gauthier-Villars, 1885.

[2] R.H. Chen and Y.M. Chiu, *Model tests of geocell retaining structures*, Geotextiles Geomemb. **26** (2008), no. 1, 56–70.

[3] R.H. Chen, Y.W. Huang, and F.C. Huang, *Confinement effect of geocells on sand samples under triaxial compression*, Geotextiles Geomemb. **37** (2013), no. 1, 35–44.

[4] S.K. Dash, K. Rajagopal, and N.R. Krishnaswamy, *Behaviour of geocell reinforced sand beds under strip loading*, Canad. Geotech. J. **44** (2007), no. 7, 905–916.

[5] A. Fakher and C.J.F.P. Jones, *When the bending stiffness of geosynthetic reinforcement is important*, Geosynth. Int. **8** (2001), no. 5, 445–460.

[6] A. Gao and M. Zhang, *Performance and application of geocell reinforced sand embankment under static and cyclic loading*, Coatings **12** (2022), no. 6, 767.

[7] A.M. Hegde and T.G. Sitharam, *Three-dimensional numerical analysis of geocell-reinforced soft clay beds by considering the actual geometry of geocell pockets*, Canad. Geotech. J. **52** (2015), no. 9, 1396–1407.

[8] M. Honardar and M.A. Roshanzamir, *Numerical analysis of effective parameters on loading capacity of strip footings placed adjacent to reinforced and unreinforced sand slopes under eccentric loading*, 1st Nat. Conf. Architect. Civil Projects Sustain. Dev. Tabris, Tabriz, Iran, 2013. [In Persian]

[9] B. Lazhar, B. Hacene, and Y. Jarir, *Internal stability analysis of reinforced earth retaining walls*, Geotech. Geol. Eng. **29** (2011), 443–452.

[10] B. Leshchinsky, *Effects of geocell confinement on strength and deformation behavior of gravel*, J. Geotech. Geoenviron. Eng. **139** (2012), no. 2, 340–352.

[11] B. Mehdipour, H. Hashemolhosseini, B. Nadi, and M. Mirmohamadsadeghi, *Investigating the effect of geocell changes on slope stability in unsaturated soil*, Tehnički Glasnik **14** (2020), no. 1, 66–75.

[12] M. Oghabi and A.K. Eisazaadeh, *Geocell reinforcement in sand and its effect on the bearing capacity*, Geotech. Res. **1** (2013), no. 3, 123–132.

[13] S. Qorbanbeigi and H. Emadollahyari, *Numerical analysis of foundations placed on shield-stabilized slopes*, Proc. 1st Nat. Civil Engin. Dev. Conf., Zibakenar, Iran, 2011, pp. 1–10. [In Persian]

[14] G.D. Skinner and R.K. Rowe, *Design and behaviour of a geosynthetic reinforced retaining wall and bridge abutment on a yielding foundation*, Geotextiles Geomem. **23** (2005), no. 3, 234–260.

[15] K. Terzaghi, *Expanded Prandtl's (1921) theory about the dimension of strip footing*, J. Soil Mech. Found. Div. **69** (1943), no. 2, 1–34.

[16] L. Zhang, M.H. Zhao, X.W. Zou, and H. Zhao, *Deformation analysis of geocell reinforcement using Winkler model*, Comput. Geotech. **36** (2009), no. 6, 977–983.

[17] L. Zhang, M.H. Zhao, X.W. Zou, and H. Zhao, *Analysis of geocell reinforced mattress with consideration of horizontal vertical coupling*, Comput. Geotech. **37** (2010), no. 6, 748–756.

[18] J.G. Zornberg and F. Arriaga, *Strain distribution within geosynthetic-reinforced slopes*, J. Geotech. Geoenviron. Eng. **129** (2003), no. 1, 32–45.